

---

# Transformations between deep neural networks

---

**Tom Bertalan**

Department of Chemical and Biomolecular Engineering  
Johns Hopkins University  
Baltimore, MD

**Felix Dietrich**

Department of Informatics  
Technical University of Munich  
Munich, Germany

**Ioannis G. Kevrekidis**

Departments of Chemical and Biomolecular Engineering &  
Applied Mathematics and Statistics  
Johns Hopkins University  
Baltimore, MD  
yannisk@jhu.edu

## Abstract

We propose to test, and when possible establish, an equivalence between two different artificial neural networks by attempting to construct a data-driven transformation between them, using manifold-learning techniques. In particular, we employ diffusion maps with a Mahalanobis-like metric. If the construction succeeds, the two networks can be thought of as belonging to the same equivalence class. We first discuss transformation functions between only the *outputs* of the two networks; we then also consider transformations that take into account outputs (activations) of a number of internal neurons from each network. In general, Whitney’s theorem dictates the number of measurements from one of the networks required to reconstruct each and every feature of the second network. The construction of the transformation function relies on a consistent, *intrinsic* representation of the network input space. We illustrate our algorithm by matching neural network pairs trained to learn (a) observations of scalar functions; (b) observations of two-dimensional vector fields; and (c) representations of images of a moving three-dimensional object (a rotating horse). The construction of such equivalence classes across different network instantiations clearly relates to transfer learning. We also expect that it will be valuable in establishing equivalence between different Machine Learning-based models of the same phenomenon observed through different instruments and by different research groups.

## 1 Introduction

In our Big Data era, and as the interactions between physics-based modeling and data-driven modeling intensify, we will be encountering—with increasing frequency—situations where different researchers arrive at different data-driven models of the same phenomenon, even if they use the same training data. The same neural network, trained by the same research group, on the same data, with the same choice of inputs and outputs, the same loss function and even the same training algorithm—but just different initial conditions and/or different random seeds, will give different learned networks, even though their outputs may be practically indistinguishable on the training set. This becomes much more interesting when the same phenomenon is observed through different sensors, and one learns a predictive model of the same phenomenon but based on different input variables—how will we realize that two very different predictive models of the same phenomenon “have learned the same thing”? In other words, how can we establish, in a data-driven way that two models are

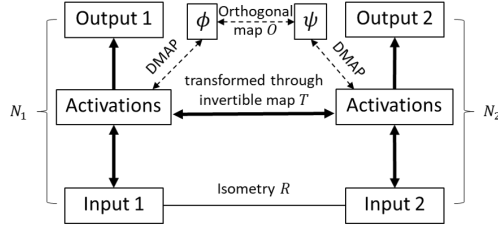


Figure 1: Transformation  $T$  between the activation spaces of two neural networks (with, in general, different inputs). The networks  $N_1, N_2$  are not necessarily invertible as maps from input to output, but all other maps shown (input isometry  $R$ , orthogonal map  $O$  between intrinsic Mahalanobis Diffusion Map spaces, Mahalanobis Diffusion Maps  $\phi, \psi$ , and the transformation  $T$ ) are invertible.

transformations of each other? The problem then becomes: if we suspect that two neural networks embody models of the same phenomenon, how do we test this hypothesis? How do we establish the invertible, smooth transformation that embodies this equivalence? And, in a second stage, can we test how far (in input space) this transformation will successfully generalize? Our goal is to implement and demonstrate a data-driven approach to establishing “when two neural networks have learned the same thing” as our title indicates: the types of observations of the networks that can be used, and an algorithm that allows us to construct and test the transformation between them. Our work is based on nonlinear manifold learning techniques, and, in particular, Diffusion Maps using a Mahalanobis-like metric [Singer et al., 2009, Berry and Sauer, 2015, Dsilva et al., 2016]. This is an attempt at “gauge invariant data mining”—processing observations in a way that maps them to an intrinsic description, where the transformation between different models is easy to perform (in our case, it can be a simple, orthogonal transformation between intrinsic descriptions). In effect, we construct data-driven nonlinear observers of each network based on the other network. We remind the reader that when we talk about “observations of the networks”, we do not mean their parameters after training; we mean observations of the “action” of the trained networks on input data: (some of) the resulting internal activations. These observations can be based on either output neurons or internal neurons of the networks, which we assume to be smooth functions over a finite dimensional input manifold. Whitney’s theorem then guides us in selecting an upper bound on how many of these functions are needed to preserve the manifold topology, and to embed the input manifold itself [Whitney, 1936].

We now briefly introduce the concept of transformations between neural networks. Details of the approach can be found in section 3 (also see figure 1). In general, we proceed as follows: **(1)** Two smooth functions, the tasks  $f_1$  and  $f_2$ , are defined on the same data set (for example, two separate denoising tasks defined on the same set of images). We will also, importantly, discuss cases of tasks defined on different data sets. In that case, when each data set lives on a separate (but assumed diffeomorphic) manifold, we will discuss conditions that enable our construction, turning the diffeomorphism into an isometry. **(2)** We separately train two networks to approximate the tasks (for example, two deep, convolutional, denoising auto-encoder networks). **(3)** Then, we use the output of “a few” internal neurons of each of the networks as an embedding space for the input manifold; the minimum number is dictated through Whitney’s theorem; **(4)** Using the Mahalanobis metric (see §3.2 for details) in a Diffusion Map kernel applied to these internal “intermediate outputs” yields two *intrinsic embeddings* of them that agree up to an orthogonal transformation  $O$ ; **(5)** The transformation between activations of the two networks can then be defined through  $T = \psi^{-1} \circ O \circ \phi$  (see figure 1), i.e., we map from the selected activations of network 1 into (a) the (Mahalanobis) Diffusion Map representation of these activations with  $\phi$ , then (b) map through an orthogonal transformation  $O$  to the Diffusion Map representation of network 2 activations, and then finally (c) invert the network 2 Diffusion Map  $\psi$  to obtain the activations of network 2 (see figure 1). Since the selected neurons are enough to embed the input manifold, all other internal (or final output layer) activations can be then approximated as functions on the embedding.

## 2 Related work

With the advent of accessible large-scale SIMD processors and GPUs, efficient backpropagation, and the wider adoption of “twists” like ReLU activations, dropout, and convolutional architectures, neural networks and AI/ML research in general experienced a “third spring” in the early 2000s, which is still going strong today. While the bulk of the work was in supervised methods, this boom also led to greater interest in unsupervised learning methods, in particular highly fruitful new work on neural generative modelling. Kingma and Welling [2014] and later Salimans et al. [2015] began this thread with their work on variational autoencoders (VAEs), which upgrade traditional autoencoders to generative models. Different autoencoders, trained on observations of the same system, will give very different latent spaces; these can be thought of as different parametrizations of the same manifold. Variational autoencoders are then a way to “harmonize” several different autoencoders, by enforcing the same prior (distribution over the latent variables). In Goodfellow et al. [2014], the “adversarial learning” framework was applied to the VAE task, with separate generator and discriminator networks being trained. This work was significantly extended by Arjovsky et al. [2017]. The idea of establishing a correspondence between different learned representations also motivates our work. Broadly, we construct invertible transformations between different sets of observations arising from activations of different neural networks. When the construction is successful, we can state that “the networks have learned the same task” over our data set; we can then explore the generalization of these transformations beyond the training set.

The idea of a transformation between systems has been broadly utilized in the manifold learning community following the seminal paper by Singer and Coifman [2008]. Berry and Sauer [2015] discuss the possibility to represent arbitrary diffeomorphisms between manifolds using such a kernel approach. Both papers employ the diffusion map framework [Coifman and Lafon, 2006]. Recently, a paper on a neural network approach for such isometries was uploaded to arXiv [Peterfreund et al., 2020], as an alternative to diffusion maps (see also the works of McQueen et al. [2016], Schwartz and Talmon [2019] for approximations of isometries).

## 3 Transformations between artificial neural networks

Here, we introduce mathematical notation, define the problem, and then illustrate the approach through examples of increasing complexity. We also introduce the concept of using the Mahalanobis metric with Diffusion Maps to construct the transformation, and discuss its use for neural networks.

### 3.1 Mathematical notation and problem formulation

We start by defining two smooth functions, the tasks  $f_1 : \mathcal{M} \rightarrow \mathbb{R}^m$  and  $f_2 : \mathcal{M} \rightarrow \mathbb{R}^m$ , with  $m \in \mathbb{N}$ . The input domain of both tasks is the manifold  $\mathcal{M}$ . We assume that  $(\mathcal{M}, g)$  is a compact,  $d$ -dimensional Riemannian manifold, embedded in Euclidean space  $\mathcal{M} \subseteq \mathbb{R}^k$ ,  $k \geq d$ , with  $g$  the metric induced by the embedding. In our first example  $\mathcal{M}$  is simply  $[-1, 1]$  and the metric is just the Euclidean metric on  $\mathbb{R}$ ; it is only later, when we want to transform between networks defined on different manifolds, that considerations of the (possibly different) metrics on these manifolds become important, since our Mahalanobis approach is based on neighborhoods of the data points. We will then write  $\text{vol}_g$  for the volume form on  $\mathcal{M}$  induced by  $g$ , and write  $\mu$  for a given, fixed measure on  $\mathcal{M}$  (the “sampling measure”), which we assume to be absolutely continuous with respect to  $\text{vol}_g$  and normalized so that  $\mu(\mathcal{M}) = 1$ . We assume that the measure  $\mu$  has a density  $\rho : \mathcal{M} \rightarrow \mathbb{R}^+$ ,  $\mu = \rho \text{vol}_g$ , that is bounded away from zero on our compact manifold  $\mathcal{M}$ . That means sampling points through  $\mu$  “covers the manifold well”.

Let  $D = \{x \in \mathbb{R}^k\} \subset \mathcal{M}$  be a finite collection of points on  $\mathcal{M}$ , sampled from the measure  $\mu$ ; for our first example, this is just the uniform measure on  $[-1, 1]$ . Two artificial neural networks  $N_1 : \mathbb{R}^k \rightarrow \mathbb{R}^m$ ,  $N_2 : \mathbb{R}^k \rightarrow \mathbb{R}^m$  approximate respectively the tasks  $f_1$  and  $f_2$ , such that for all  $x \in D$ ,  $N_1(x) \approx f_1(x)$ ,  $N_2(x) \approx f_2(x)$ . We purposefully omit assumptions on how the two networks generalize for data not contained in  $D$ , because we want to test these generalization properties later. We will later also discuss how to transform between networks trained on different input datasets.

We then consider the output of every individual neuron in the two networks as a real valued function on the  $d$ -dimensional input manifold. If every layer has at least  $2d + 1$  neurons, the topology of the

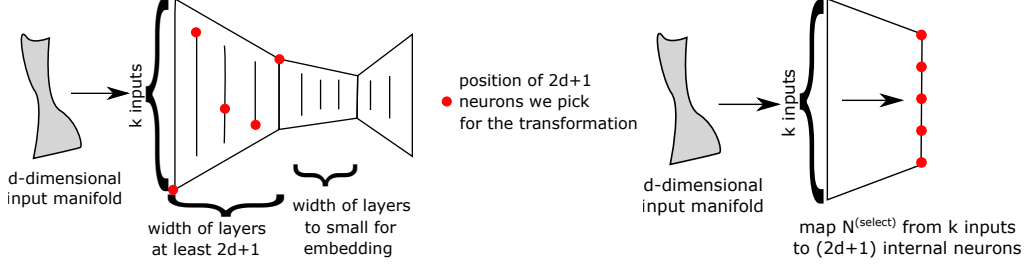


Figure 2: Left: Network layout and selection of  $\ell \geq 2d + 1$  neurons in the first part of the network (where all layers have enough neurons to embed the  $d$ -dimensional input manifold  $\mathcal{M}$ ). The activations of the  $\ell$  neurons contain enough information to map (a) to the activation of any other neuron, or (b) to any neuron of another network defined on the same manifold. Right: the map  $N^{(\text{select})}$ , from the same  $k$  inputs as the network, to the  $\ell$  internal neurons (the red dots on the left).

input manifold will, generically, be preserved while it is passed from layer to layer. In this case, all neurons everywhere in the network can be considered generic observables of the input manifold, and so picking any  $2d + 1$  of them as coordinates is enough to create an embedding space for the input manifold.

This means that our transformation function can map from any  $2d + 1$  neurons in one network to any  $2d + 1$  neurons in the other network, invertibly, for data on the manifold.

As an illustration of the theoretical concept, consider a line segment  $\mathcal{M} = [-1, 1]$ . If we pick a single polynomial  $p(x) = (x - 2a)x$  with the parameter  $a$  chosen randomly in  $(-1, 1)$ , it cannot be used as an embedding of  $\mathcal{M}$ , because it folds over at the point  $x = a$ . However, if we pick three of these random polynomials as three new coordinates for  $\mathcal{M}$ , then  $(p_1(\mathcal{M}), p_2(\mathcal{M}), p_3(\mathcal{M}))$  is an embedding of  $\mathcal{M}$  into  $\mathbb{R}^3$  almost surely (i.e. with probability one). The fact that this holds for arbitrary smooth manifolds  $\mathcal{M}$  and  $2d + 1$  coordinates follows from the work of Whitney [1936], with probabilistic arguments by Sauer et al. [1991].  $2d + 1$  generic observations provide a guarantee; if one is lucky, one may be able to create a useful embedding with less (but of course at least  $d!$ ) observations.

In general, if any layer (in particular, the output) of a network has less than  $2d + 1$  neurons, (or if, say, several weights become identically zero so that the output of several neurons in a layer is constant, and no longer a generic function over the input) then the topology of the input manifold may not be preserved, and the manifold will be “folded” or “collapsed”. In this case, a transformation to the other network is no longer possible when we only use observations of neurons in or after that layer. We demonstrate this in §4.1.

We will write  $N_i^{(\text{select})} : \mathbb{R}^k \rightarrow \mathbb{R}^\ell$  for the map of the input of network  $i = 1, 2$  to  $\ell \geq 2d + 1$  internal neurons that we select for our transformation, and  $N_i : \mathbb{R}^k \rightarrow \mathbb{R}^m$  for the mapping from the input to the output. These  $\ell$  neurons must constitute generic observations of the input manifold; they can in principle lie at any internal (some possibly even at the input or output) layer. Figure 2 illustrates that in the network we can pick (red) neurons as the output of our map  $N_i^{(\text{select})}$  only in layers where all previous layers have at least  $2d + 1$  neurons.

The problem of finding transformations between neural networks can now be formulated as follows.

**Definition 1.** *Based on output data only. Construct an invertible map  $T_A : \mathbb{R}^m \rightarrow \mathbb{R}^m$  such that  $\forall x \in D$ ,*

$$(T_A \circ N_1)(x) = N_2(x).$$

**Definition 2.** *Based on internal activation data. Construct an invertible map  $T_B : \mathbb{R}^\ell \rightarrow \mathbb{R}^\ell$ , with  $\ell \geq 2d + 1$ , such that  $\forall x \in D$ ,*

$$(T_B \circ N_1^{(\text{select})})(x) = N_2^{(\text{select})}(x).$$

**Definition 3.** *Different input data. Assume the tasks  $f_1$  and  $f_2$  are defined on two isometric Riemannian manifolds  $(\mathcal{M}, g_1)$  and  $(\mathcal{M}, g_2)$  (such that there exists an isometry  $R : \mathcal{M} \rightarrow \mathcal{M}$  with  $R_*g_1 = g_2$ ). Construct the map  $T_B : \mathbb{R}^\ell \rightarrow \mathbb{R}^\ell$ ,  $\ell \geq 2d + 1$ , such that for  $\forall x \in D$ ,*

$$(T_B \circ N_1^{(\text{select})})(x) = (N_2^{(\text{select})} \circ R)(x).$$

Here,  $R_*g_1$  denotes the push-forward of the metric  $g_1$  by  $R$ .

### 3.2 Constructing the transformation

In this section, we explain how to construct the transformation between the networks in a consistent way. The crucial step in our approach is to employ spectral representations of the internal activation space of the two networks. These representations are constructed through manifold learning techniques introduced by Singer and Coifman [2008], Berry and Sauer [2015]: Given a metric  $g$  and its push-forward metric  $S_*g$  by a diffeomorphism  $S : \mathcal{M} \rightarrow \mathcal{M}$ , the map  $S$  can be reconstructed up to a linear, orthogonal map. The reconstruction can even be done in a data-driven way, employing diffusion map embeddings [Coifman and Lafon, 2006] and a so-called ‘‘Mahalanobis distance’’ [Singer and Coifman, 2008, Dsilva et al., 2016].

The diffusion maps algorithm utilizing the Mahalanobis distance is described in algorithm 1. We often only have non-linear observations of points on the manifold  $\mathcal{M}$ , given by an observation function  $S : \mathcal{M} \rightarrow \mathbb{R}^m$ . In our case, the tasks  $f_1, f_2$  and in particular the neural network maps  $N_i^{\text{select}}$  provide such non-linear observations of the input manifold  $\mathcal{M}$ . Such maps usually distort the metric on  $\mathcal{M}$ , so that the original geometry is not preserved. We can still parametrize  $\mathcal{M}$  with its original geometry if we employ the following approach: In the kernel used by the Mahalanobis Diffusion Map algorithm, the similarity between points includes information about the observation functions  $S$  (here, the  $N_i^{\text{select}}$ ) that have to be invertible on their image. For  $y_i, y_j \in S(\mathcal{M}) \subset \mathbb{R}^m$ ,

$$d_M^2(y_i, y_j) = (y_i - y_j)^T (J^T(y_i)J(y_i) + J^T(y_j)J(y_j)) (y_j - y_i), \quad (1)$$

$$k(y_i, y_j) = \exp\left(-\frac{d_M^2(y_i, y_j)}{2\varepsilon}\right), \quad (2)$$

where  $J(y)$  is the Jacobian matrix of the inverse transformation  $S^{-1}$  at the point  $y$ . The product  $J^T J$ , on which the entire procedure hinges, can be approximated through observations of data point neighborhoods: typically in the form of a covariance, obtained, for example, by short bursts of a stochastic dynamical system on  $\mathcal{M}$ , subsequently observed through  $S$  [Singer et al., 2009]. In algorithm 1, we do not specify how the neighborhoods for the computation of the covariance matrix are obtained. We do so separately for each of the computational experiments in section 4 (see also the discussion by Dietrich et al. [2020]).

The reconstruction of the eigenspace up to an orthogonal map is justified through the following argument from Moosmüller et al. [2020]: using the distance (1) is effectively using the metric  $S_*g$  on the data, turning  $S$  into an isometry. Laplace-Beltrami operators of isometric manifolds have the same eigenvalues, and in that case eigenfunctions associated to the same eigenvalue are related by an orthogonal map [Berry and Sauer, 2015, Rosenberg, 1997]. Therefore, an isometry  $S$  between the base manifolds  $(\mathcal{M}, g)$  and  $(\mathcal{M}, S_*g)$  turns into an orthogonal map in eigenfunction coordinates of the manifolds [Berry and Sauer, 2015].

Finally, to construct the transformation between neural networks using the diffusion map approach, we proceed as described in algorithm 2. Essentially, we generate embeddings of the input manifolds of the two networks using their internal neurons, and then employ algorithm 1 to construct a consistent representation for each of these embeddings. Since these representations are invariant up to an orthogonal map, we can construct our transformation after estimating this final map, which only requires a small number of ‘‘common measurements’’ (it is easier to parametrize linear maps than general nonlinear ones!).

## 4 Demonstrating transformations between neural networks

We now demonstrate the transformation concept in three separate examples. Section 4.1 illustrates a simple transformation between two networks with the same one-dimensional input, trained on the same task. Section 4.2 then broadens the scope to networks trained on different one-dimensional inputs. Section 4.3 shows how to construct a transformation using observations of internal activations of two networks defined on two-dimensional spaces. Section 4.4 describes our most intricate example, with images as input for two deep auto-encoder networks with several convolutional layers. We show how to map between internal activations of these networks and how to reconstruct the output of one network from the input of the other. Table 1 contains metrics and parameters for the computational experiments.

---

**Algorithm 1:** Diffusion maps algorithm, using the Mahalanobis-metric [Singer et al., 2009] (and the similarity transform from Berry et al. [2013]).

---

**Input:**  $n \in \mathbb{N}$ : Number of neighborhoods.  $m \in \mathbb{N}$ : Dimension of points in the input.  $q \in \mathbb{N}$ : Number of points per neighborhood.  $\ell \in \mathbb{N}$ : Number of eigenvectors to compute.  $Y$ : Set of  $n$  neighborhoods  $Y_i = \{y_i^{(j)} \in \mathbb{R}^m\}, i = 1, \dots, n, j = 1, \dots, q$ .

1. Compute inverse covariance matrices  $C_i = \text{cov}(Y_i)^{-1} \in \mathbb{R}^{m \times m}, i = 1, \dots, n$ .
2. Compute kernel matrix  $K \in \mathbb{R}^{n \times n}$  through equation (2), using the approximation  $J(\mathbb{E}[Y_i])^T J(\mathbb{E}[Y_i]) \approx C_i$  and kernel bandwidth  $\epsilon$  through median of squared Mahalanobis-distances to  $k$ -th nearest neighbor of all points, where we choose  $k = 10$ .
3. Normalize kernel matrix to make it invariant to sampling density:
  - (a) Form the kernel matrix  $W = P^{-1} K P^{-1}$ , with diagonal matrix  $P_{ii} = \sum_{j=1}^N K_{ij}$ .
  - (b) Form the matrix  $\hat{T} = Q^{-1/2} W Q^{-1/2}$  with diagonal matrix  $Q_{ii} = \sum_{j=1}^N W_{ij}$ .
  - (c) Find the  $\ell$  largest eigenvalues  $a_p$  associated to non-harmonic eigenvectors  $v_p$  of  $\hat{T}$ . See Dsilva et al. [2018] for a discussion and method to remove harmonic eigenvectors.
  - (d) Compute the eigenvalues of  $\hat{T}^{1/\epsilon}$  by  $\lambda_p = a_p^{1/(2\epsilon)}$ .
  - (e) Compute the eigenvectors  $\phi_p$  of the matrix  $T = Q^{-1} W$  through  $\phi_p = Q^{-1/2} v_p$ .
4. Define diffusion map  $\phi : \mathbb{R}^m \rightarrow \mathbb{R}^\ell$  and its inverse through interpolation (here: nearest neighbor interpolation. More advanced techniques such as Nyström extension [Chiavazzo et al., 2014] or neural networks are also possible—this is a supervised learning problem).

**Output:**  $\phi : \mathbb{R}^m \rightarrow \mathbb{R}^\ell$ : diffusion map from the input space to  $\ell$  eigenvectors.

---



---

**Algorithm 2:** Algorithm to compute the transformation between two neural networks.

---

**Input:**  $\ell \geq 2d + 1$ : Number of neurons to use from both networks  $N_1, N_2$ .  $\ell$  is also the number of eigenvectors we use for the spectral embedding.  $S_1, S_2 : \mathcal{M} \rightarrow \mathbb{R}^{\ell \times q}$ : Sampling procedures of neighborhoods, consisting of  $q \in \mathbb{N}$  points each, on the input manifolds.  $n_1, n_2 \in \mathbb{N}$ : Numbers of neighborhoods to sample using  $S_1, S_2$ .

1. Sample sets of neighborhoods  $\mathcal{X}_1 = \{S_1(i)\}_{i=1}^{n_1}$ , and  $\mathcal{X}_2 = \{S_2(i)\}_{i=1}^{n_2}$ .
2. Evaluate the networks  $N_1, N_2$  separately on all points in their sets of  $\mathcal{X}_1, \mathcal{X}_2$  and record the output of the  $m$  selected neurons in sets of neighborhoods  $\mathcal{Y}_1, \mathcal{Y}_2$ .
3. Use the neighborhoods in  $\mathcal{Y}_1, \mathcal{Y}_2$  for algorithm (1) to construct invertible maps  $\phi, \psi$  from data of the  $m$  neurons of  $N_1, N_2$  to the embedding into  $\ell$  eigenvectors (see algorithm 1).
4. There is only an orthonormal transformation  $O \in SO(\ell)$  missing between the two sets of eigenvectors. Here, we estimate it with a few known corresponding points. Alternatives include the use of an iterative closest point algorithm [Rusinkiewicz and Levoy, 2001] or Procrustes alignment methods, e.g. [Kabsch, 1976].
5. Construct the map  $T$  through  $y_2 = T(y_1) = \psi^{-1} \circ O \circ \phi(y_1)$ .

**Output:** Invertible map  $T : \mathbb{R}^\ell \rightarrow \mathbb{R}^\ell$  from  $\ell$  neurons in network  $N_1$  to  $\ell$  neurons in  $N_2$ .

---

Table 1: Data and parameters of computational experiments. If not otherwise specified, we use the same parameters for both networks in a column; otherwise, different network hyperparameters are given on different lines. Activation functions are tanh except for §4.4, as described in the text.

Experiment	§ 4.1	§ 4.2	§ 4.3	§ 4.4
# Training	10,240	900	3,600	1,943 (at 64×64 resolution)
# Validation	512	100	400	216
Training Error	$5.7 \cdot 10^{-6}$ $2.0 \cdot 10^{-5}$	$1.48 \cdot 10^{-5}$ $8.60 \cdot 10^{-3}$	$7.3 \cdot 10^{-5}$ $2.5 \cdot 10^{-6}$	$1.2 \cdot 10^{-1}$ $1.1 \cdot 10^{-1}$
Validation Error	$1.4 \cdot 10^{-1}$ $1.0 \cdot 10^{-1}$	$1.58 \cdot 10^{-5}$ $5.66 \cdot 10^{-3}$	$4.6 \cdot 10^{-5}$ $2.4 \cdot 10^{-6}$	$2.6 \cdot 10^{-1}$ $1.1 \cdot 10^{-1}$
Architecture	1-1-1, 1-8-8-8-1	1-3-1	2-5-5-5-5-2	CNN (see text)
$q$ : Nbfd. size	1,024	11	(analytic covariance)	431
$n$ : # Nbhds.	512	990	100,000	649
$\epsilon$ : Kernel bandwidth	$1.33 \cdot 10^1$ $5.54 \cdot 10^1$	5	$1.21 \cdot 10^{-3}$ $8.06 \cdot 10^{-4}$	$9.68 \cdot 10^0$ $1.33 \cdot 10^1$

#### 4.1 Transformations between output layers of simple networks

In this first example, we demonstrate the idea of transformations between neural networks in a very simple caricature: Two tasks  $f_1, f_2 : \mathcal{M} \rightarrow \mathbb{R}$  with  $\mathcal{M} = [-1, 1] \subset \mathbb{R}$ , are approximated by two neural networks  $N_1, N_2$ . We choose the tasks to be identical,  $f_1 = f_2 = f$ , and defined by  $f(x) = -x^2$ . The training data set for the two networks is also the same,  $D_1 = D_2 = D \subset [-1, 0]$ . We follow algorithm 2 to construct the map  $T : \mathbb{R} \rightarrow \mathbb{R}$  between the one-dimensional output of both networks. The local neighborhoods  $Y_i$  of points in the training domain  $D_1$  are generated through  $\delta$ -balls around each point, with  $\delta = 0.05$ .

Figure 3(a) shows the task  $f$  as well as the evaluations of the two networks on the training data in  $[-1, 0]$  as well as their extrapolation to all of  $\mathcal{M}$ . The networks approximate  $f$  well on the training data, but extrapolate differently beyond it. This extrapolation issue is further illustrated in Fig. 3(b), where we can see that it is impossible to map from network  $N_2$  back to network  $N_1$  over all of  $\mathcal{M}$ , because the output of  $N_2$  is not an invertible function of the output of  $N_1$  over all of  $\mathcal{M}$ . However, if we use as observables the one or eight neuron(s) in the final hidden layers of the two networks (see Fig. 4(a), and architectures in Table 1), we can easily construct the transformation over all of  $\mathcal{M}$  using algorithm 2 (for the result see Fig. 4(b)). Fig. 4(c) shows the reconstruction of the selected neuron activations of Network 2 based on our transformation and our Network 1 activation observations. It is worth noting that *any* other activation of Network 2 neurons can be also approximated through, e.g. Geometric Harmonics as functions of the intrinsic representation; other types of approximation of these functions (e.g. neural networks or Gaussian Processes, or even just nearest neighbor interpolation) are also possible. For the purposes of Fig. 4(c), we compute  $\psi^{-1}$  through univariate, linear interpolation. Note that for Network 1 we can “get by” with a single observation and not the “guaranteed”  $2 \times 1 + 1 = 3$  observations: the architecture and the activation function are so simple that this single observation is one-to-one with the single input (does not “fold” over the input).

#### 4.2 Transformation between internal neurons of networks with different inputs

Here, we demonstrate the transformation concept through a simple mapping between two networks trained on the same task, but with *different*, albeit still one-dimensional inputs. This is similar to experiment §4.3, but in a much lower-dimensional ambient space, where we can easily visualize all embeddings. Table 1 contains metrics and parameters for this example.

Define tasks  $f_1, f_2$  identical to  $f : \mathbb{R} \rightarrow \mathbb{R}$  with  $f(x) = -(x - 0.25)^2 - 1$ . We use training data  $D_1 \in [0, 1]$  and  $D_2 \in [2, 4]$ , which are related by the nonlinear transformation  $S(x) = 2 + 2x + \sin(4\pi x)/(3\pi)$  (see figure 5). This transformation *is not an isometry*, but we assume that we have access to neighborhoods created by sampling in domain 1, and then transforming to domain 2 through  $S$  (see figure 5).

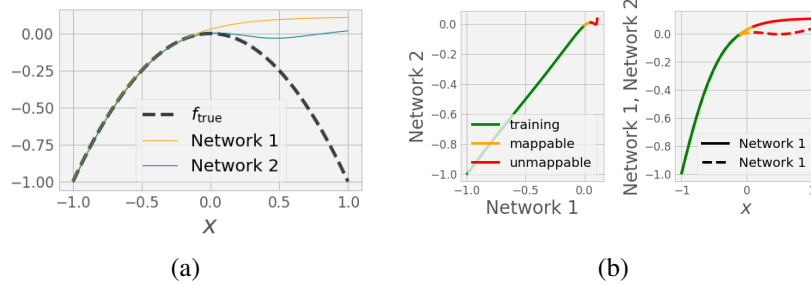


Figure 3: (a) Two networks  $N_1$  and  $N_2$  fitted to the left half of a parabola (dashed).  $N_1$  has one hidden tanh neuron, and so is strictly monotonic w.r.t. the input  $x$ , and  $N_2$  has 24 neurons in three hidden layers. (b) Output of the two networks plotted against each other. They can be mapped invertibly within the training data (green) as well as in a small neighborhood beyond (yellow).

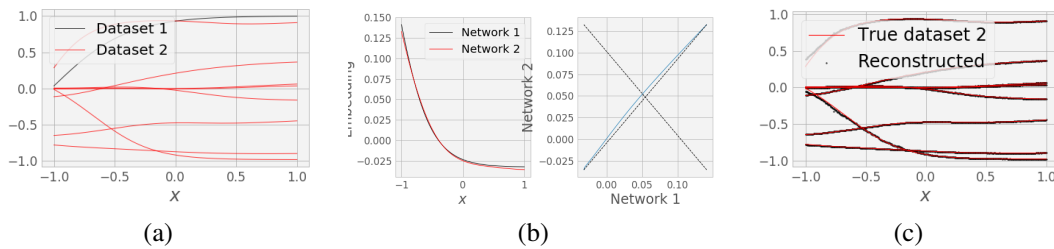


Figure 4: (a) Activations of neurons in the hidden layers of the two networks, evaluated beyond the training region. Dataset 1 contains the activations of the single hidden neuron in  $N_1$ ; dataset 2 contains the activations of the last hidden layer of  $N_2$ . (b) Separately embedding the two datasets with diffusion maps (and Mahalanobis scaling) results in coordinates that are related by an orthogonal transformation (in one dimension, multiplication by  $\pm 1$ ). (c) Our selected activations from the second network, reconstructed as functions of the selected activations from the first network.

The neural networks  $N_1, N_2 : \mathbb{R} \rightarrow \mathbb{R}$  approximate the task well on their training data (see figure 6). To construct the transformation between their internal neurons, we sample small neighborhoods of 15 points for each data point on the domains of the two networks (inside, but also far outside the training data set, on  $[0, 4]$ ). The neighborhoods on the domain of the second network are created by transforming points on the domain of the first through  $S$ . It is important to note that the data for our construction of the transformation between the two networks do not need to be evaluated at exactly “corresponding points”, obtained from each other through  $S$ ; correctly sampled neighborhoods are enough. That means we do not even need access to the map  $S$ , in principle, as long as we are given correct neighborhood information around each point by any other means, e.g. through a consistent sampling procedure Singer et al. [2009], Dietrich et al. [2020], Moosmüller et al. [2020]. We then compute covariance matrices in the space of some triplets of internal neurons of the networks, after evaluating the networks on each point within every data point neighborhood. We do not need to store the output values of the networks, just values of activations of three neurons anywhere across the network architecture is enough ( $2d + 1 = 3$  here, since the input manifold is one-dimensional). The covariance matrices are then used to construct the Mahalanobis distance between the data points. As we use three internal neurons for each network, the matrices are  $3 \times 3$  and all have rank 1. As we demonstrate in §4.2, if the inputs are isometric, the covariance matrices with respect to the inputs do not need to be generated in such a way for the approach to work: we can directly compute  $J(y)^T J(y)$  by automatically differentiating through the network.

An embedding of the activations data over the domain  $[0, 4]$  for the two networks, using diffusion maps and the Mahalanobis distance, results in an embedding of the line segment, related only by an orthogonal map (here, a flip through multiplication by  $\pm 1$ , see figure 7(c)). If we do not use the Mahalanobis distance, the embeddings of the input domain into the activation spaces of the two networks generically induce different metrics; then, even though the diffusion map algorithm will result in parametrizations of the two curves, they cannot easily be mapped to each other (figure 7(b)):



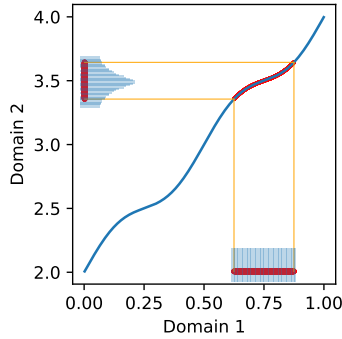


Figure 5: Uniform density in a local neighborhood on domain 1 is being transformed by the function  $S$  to non-uniform density on domain 2. Using the covariance of the neighborhoods in domain 2, we can estimate the derivative (in higher dimensions, Jacobian matrix) of the transformation function between the domains.

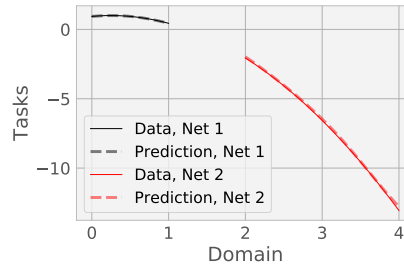


Figure 6: Setting of the computational experiment, showing tasks  $f_1, f_2 = f$  over the training data  $D_1 \in [0, 1]$  and  $S(D_1) = D_2 \in [2, 4]$ .

they are related by an arbitrary diffeomorphism, which, in general, a few corresponding points are not enough to approximate.

### 4.3 Toward more complicated networks: mapping between vector fields

We now demonstrate that we can also transform between networks that were trained to approximate vector fields on two-dimensional Euclidean space. We denote the input coordinates for network 1

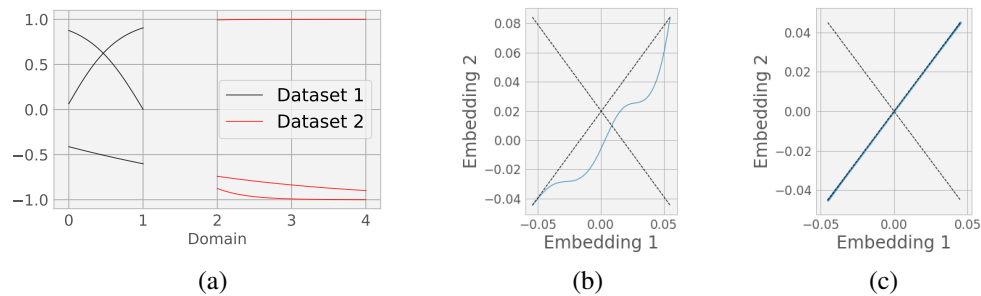


Figure 7: Panel (a): Selected activations from networks 1 and 2, used as inputs for Mahalanobis diffusion maps. Panel (b): Using Euclidean distances in the Diffusion Map kernel only recovers embeddings up to a diffeomorphism. Panel (c): Using the Mahalanobis distance recovers almost the same embedding for both networks—up to a sign in one dimension, corresponding to an orthogonal transformation in higher dimensions.

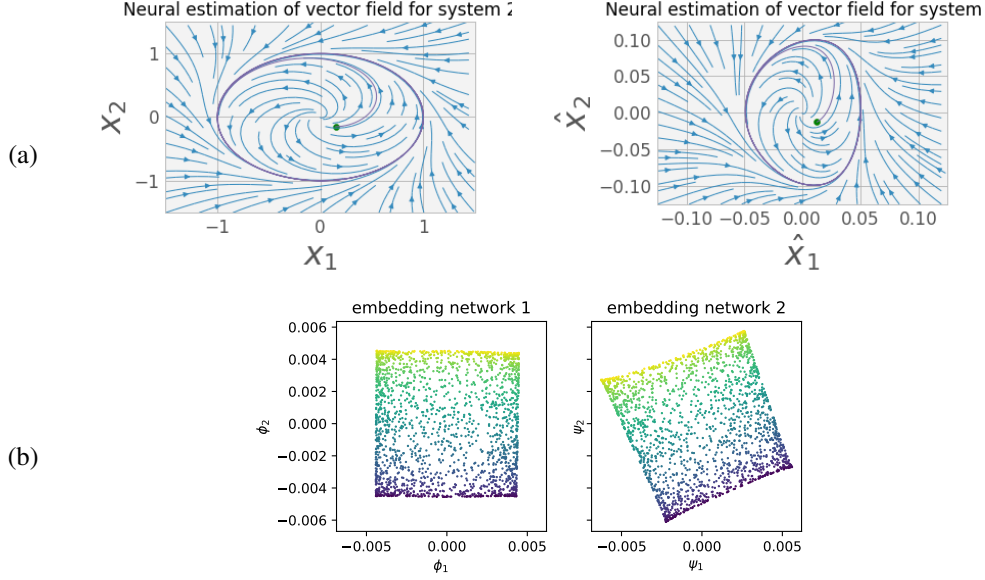


Figure 8: (a): Neural network approximations of the vector fields. (b): Embedding of the 5-dimensional activation data from the two networks from section 4.3. The covariance matrices were obtained through automatic differentiation. Each panel shows 2,000 points out of the 100,000 used for the embedding, which is consistent for both data sets, and (when ignoring some problems at the edges of the square on the right panel) differs only up to an orthogonal transformation (here, a rotation). The color corresponds to the  $x_1$  coordinate (right panel:  $\hat{x}_1$ ) in the original space.

by  $(x_1, x_2)$  and for network 2 by  $(\hat{x}_1, \hat{x}_2)$ . Figure 8(a) shows the vector fields<sup>1</sup> we use as tasks to train the neural networks. We want to demonstrate that we can construct a transformation  $T$  between activations of *internal* neurons in case the input manifold has a dimension larger than one (here: two). The input manifold for the two networks is chosen to be the same: a square  $[-1.5, 1.5]^2$  in the two-dimensional Euclidean plane, centered on the origin. The two networks are trained to map points in this two-dimensional domain to the time derivatives at those points, i.e. to coordinates of vectors (also two-dimensional). We explicitly compute the Jacobian product in the Mahalanobis distance (1), through automatic differentiation through the networks up to the (five) internal neurons of each. Densely sampling the input of both networks with 100,000 points leads to as many covariance matrices of shape  $5 \times 5$ , all of rank two (because the input space is two-dimensional). We sampled that many points to demonstrate that the approach scales well: the construction of the two spectral representations (using algorithm 1, see figure 8(b)) only took 20 minutes on a single core (Intel Core i9-9900 CPU 3.10GHz).

#### 4.4 Transformations between deep convolutional networks with high-dimensional input

In order to demonstrate our transformation between networks on a more realistic example, we generate two datasets of images  $x_i$  (high-dimensional representations) with a low-dimensional intrinsic space. Namely, we rotate a 3D model horse, and render images from two camera angles (see figure 9). For training, we additionally create augmented data by adding  $z = |\hat{z}|$  to each pixel uniformly at random,

<sup>1</sup>The vector fields used for the tasks of this experiment are defined via

$$\begin{aligned} \frac{d}{dt} \begin{pmatrix} x_1 \\ x_2 \end{pmatrix} &= \begin{pmatrix} -x_2 + x_1(1 - x_1^2 - x_2^2) \\ x_1 + x_2(1 - x_1^2 - x_2^2) \end{pmatrix}, \\ \frac{d}{dt} \begin{pmatrix} \hat{x}_1 \\ \hat{x}_2 \end{pmatrix} &= J(s^{-1}(\hat{x}_1, \hat{x}_2)) \cdot \frac{d}{dt} (s^{-1}(\hat{x}_1, \hat{x}_2)) = J(x_1, x_2) \frac{d}{dt} \begin{pmatrix} x_1 \\ x_2 \end{pmatrix}, \end{aligned} \quad (3)$$

where  $J(x_1, x_2)$  is the Jacobian matrix of the map  $(\hat{x}_1, \hat{x}_2) = s(x_1, x_2) = \left( \frac{x_1}{\alpha} + \left( \frac{x_1^2}{\alpha^2} + \frac{x_2}{\beta} \right), \frac{x_1^2}{\alpha^2} + \frac{x_2}{\beta} \right)$ , for  $\alpha = 20$  and  $\beta = 10$ .

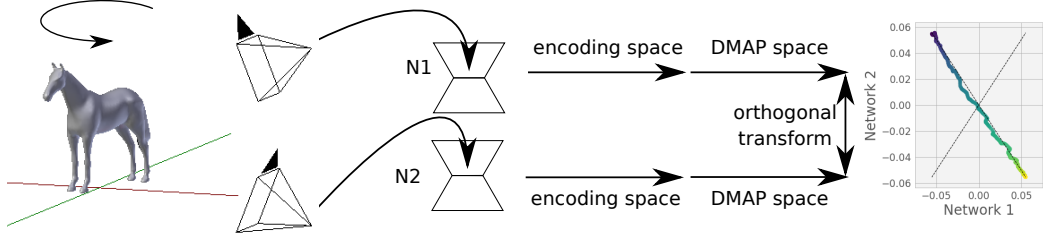


Figure 9: Setting for our example of high-dimensional input space. Two cameras observe a rotating horse. We encode the images using two deep autoencoder networks  $N_1$  and  $N_2$ , encoding the images in six dimensions. diffusion maps with the Mahalanobis distance applied to the data in this space yields a consistent embedding, invariant up to an orthogonal transformation (here, a sign flip).

where  $\hat{z} \sim \mathcal{N}(0, 1/10)$ , pixel values are chosen in  $[0, 1]$ , and we re-threshold pixels to this range after augmentation. We divide the range  $[0, 2\pi]$  of object rotation into 3,600 bins, but only train on images in  $\theta \in [\pi, 0.6\pi]$ .

The functions  $f_1$  and  $f_2$  in this example are denoising tasks for images obtained from the two cameras. To approximate them, we train two convolutional autoencoders to reconstruct the input images, with the reconstruction target being the noiseless original images when noise-augmented images are the input. We minimize a pixelwise binary cross-entropy loss, to which we add the term  $10^{-5} \cdot [(l - l^*)^2 + (h - h^*)^2]$ , where  $l$  and  $h$  are, respectively, the batchwise minimum and maximum of the bottleneck layer activations, and  $l^* = \pi$  and  $h^* = 0.6\pi$  are our desired values for this range. This pinning term does not affect any of our other results, but improves legibility of the plots.

Our encoders have interleaved two-dimensional convolutional layers ( filter sizes 9, 7, 5, 3, 3, channel counts 8, 32, 64, 16, stride of 1, and “same” padding ) and width-2 max-pooling layers in the encoding portion, followed by two width-6 dense layers to output our encodings  $y_i$ . The decoders have interleaved convolutional layers (with reversed filter sizes and channel counts to produce a pyramid of same-shape tensors) and unlearned nearest-neighbor resizing operations in the decoding portion to output tensors of the same shapes as the input. All activations are ReLU except for the final layer, which is sigmoid. We use AdaM with Nesterov momentum with a batch size of 128, for 220 epochs, with a learning rate of  $10^{-4}$ . Training generally takes less than five minutes per autoencoder on an Nvidia RTX 2080 ti GPU, with a training loss of  $1.2 \cdot 10^{-1}$  and validation loss of  $2.6 \cdot 10^{-1}$ .

We did not do any systematic hyperparameter search, and there are obvious improvements that we did not attempt to achieve better performance on the autoencoder tasks, as the network→network transformation was the actual project of interest.

In order to compute the inverse covariances  $C_i$  for the Mahalanobis distances described in algorithm 1, for each (high-dimensional) image  $x_i(\theta_i)$  we evaluate the (low-dimensional) encodings  $y_j$  for the pre-sampled images  $x_j(\theta_j)$ ,  $j = i - d, \dots, i, \dots, i + d$  to the left and to the right in  $\theta$ , where  $i$  is taken s.t.  $j$  never indexes outside the training data ( $d = (q - 1)/2$  and  $q$  is as given in Table 1). We then evaluate the covariance of this cloud of low-dimensional encodings, and use the pseudoinverse of this as  $C_i$ .

To complete the example, we compute “cross-decodings” by (1) evaluating an image  $x(\theta)$  from the first dataset on the first encoder, (2) interpolating this to its corresponding Mahalanobis diffusion map embedding, (3) finding the nearest embedding in the other network’s diffusion map, (4) interpolating this to the second network’s encoding, and finally (5) evaluating the second network’s decoder with this encoding. The result is shown in Fig. 10. When the first image is rotated by sweeping  $\theta$  through the training range (not shown here), the reconstructed second view rotates correspondingly. Note that the map from one embedding to the other is an orthogonal transformation (here, simply multiplication by  $+1$  or  $-1$ ), and can, in general, be computed as an unscaled SVD  $U \cdot V^T$ , using only a small set of correspondences (here, just two pairs of corresponding points are enough to determine the sign). This is what allowed us to perform Step 3 in “cross-decoding” above.

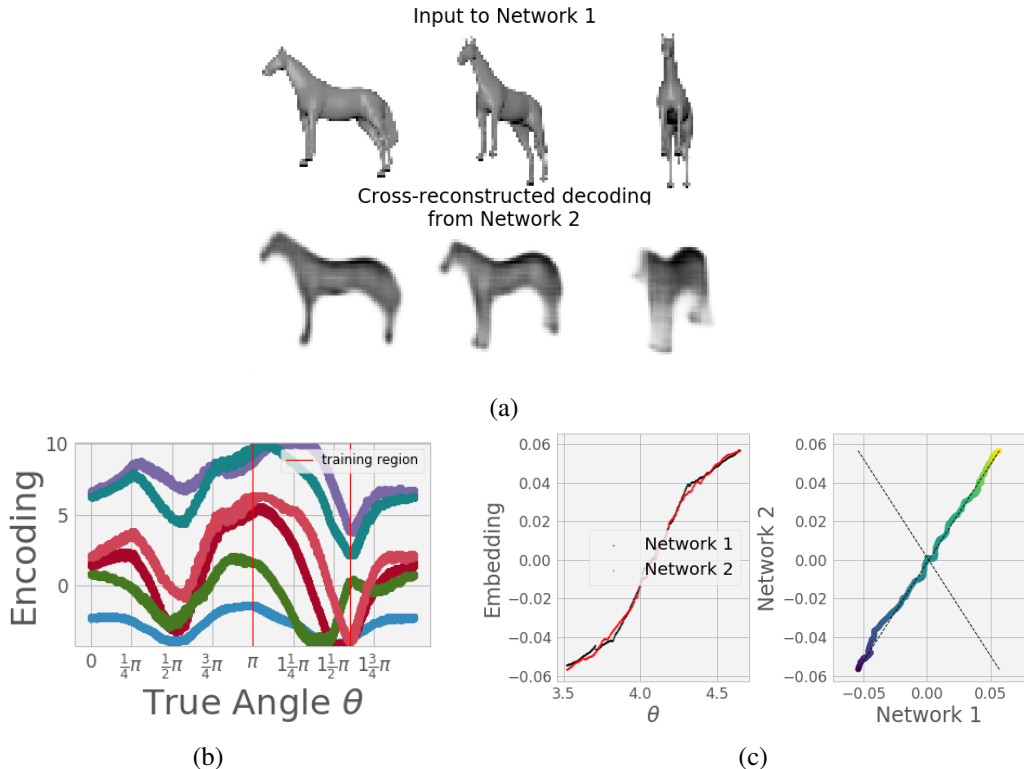


Figure 10: *Reconstructing one camera view from another.* We create a dataset of 3/5 of a complete rotation of a horse figure, viewed from above and below, and train two convolutional autoencoders on these data. We then construct two Mahalanobis diffusion maps of these encodings, find the smallest orthonormal transformation between these, and then use this chain of transformations to construct the output of one autoencoder from the input of the other.

## 5 Discussion

In this work we formulated and implemented algorithms that construct transformation functions between observations of different deep neural networks in an attempt to establish whether these networks embodied realizations of the same phenomenon or model. We considered observations of the activations of both output neurons and internal neurons of the networks; we assumed these are smooth (nonconstant!) functions over an input manifold. This allowed us to employ Whitney’s theorem as an upper bound on how many of these functions are needed to preserve the input manifold topology. With the transformation, we could map from the input of one network, through its activations and the transformation, to the state (activations) and output of the other network. We also explored the generalization properties of the networks and how our transformation fails—as we explore input space—when the observations cannot be mapped to each other any more. Our transformations go beyond the probabilistic correspondences typically imposed by VAEs, towards point-wise correspondences between manifolds.

Open challenges: **(1)** Our approach hinges on being able to observe not just a single input processed by the network, but also how a small neighborhood of this input is processed by the network. Obtaining such neighborhoods on the input manifold in a way consistent across the two networks is a nontrivial component of the work—it constitutes part of our *observation process*, of the way data used for the training of the two networks have been collected. Our work suggests that protocols for data collection that provide such additional information can be truly beneficial in model building [Moosmüller et al., 2020, Dietrich et al., 2020]; **(2)** Which internal neurons to pick for the input space embedding? In principle, any  $2d + 1$  neurons would be enough, but in practice, different choices vary widely in the curvature they induce on the embedding, leading to different numerical conditioning of the problem; **(3)** How to deal with intrinsically high-dimensional input manifolds, or

widely varying sampling densities? These would necessitate large training data sets. Recent work on Local Conformal Autoencoders [Peterfreund et al., 2020] and their empirically observed good extrapolation performance may prove helpful.

## 6 Broader Impact

The construction of transformation functions between different neural networks (and different data-driven, possibly even physically informed, models in general) has wide-ranging implications, since it enables us to calibrate different data-driven models to each other. It also holds the promise of allowing us to improve qualitatively correct (but quantitatively inaccurate) models by calibrating them to experimental data. Starting with one model and calibrating it to another is, in effect, a form of transfer learning and domain adaptation.

It may be possible to calibrate different models to each other over a large portion of input space, yet the calibration may fail for inputs far away from the training set. Our procedure allows us to explore the way this calibration (the ability to qualitatively generalize) fails, *by locating singularities in the transformation* as we move away from the training set, exploring input space. Systematically exploring the nature and onset of these singularities, and what they imply about the nature of the underlying physics is, we believe, an important frontier for data-driven modeling research.

## Acknowledgments and Disclosure of Funding

This work was partially supported by the DARPA PAI program. F.D. would also like to thank the Department of Informatics at the Technical University of Munich for their support. It is a pleasure to acknowledge discussions with Drs. J. Bello-Rivas and J. Gimlett.

## References

- Martin Arjovsky, Soumith Chintala, and Leon Bottou. Wasserstein Generative Adversarial Networks. *International Conference on Machine Learning*, page 10, 2017.
- T. Berry, J. R. Cressman, Z. Gregurić-Ferenček, and T. Sauer. Time-scale separation from diffusion-mapped delay coordinates. *SIAM Journal on Applied Dynamical Systems*, 12(2):618–649, January 2013. doi: 10.1137/12088183x.
- Tyrus Berry and Timothy Sauer. Local kernels and the geometric structure of data. *Applied and Computational Harmonic Analysis*, 40:439–469, March 2015. ISSN 1063-5203. doi: 10.1016/j.acha.2015.03.002.
- Eliodoro Chiavazzo, Charles Gear, Carmeline Dsilva, Neta Rabin, and Ioannis Kevrekidis. Reduced models in chemical kinetics via nonlinear data-mining. *Processes*, 2(1):112–140, 2014. ISSN 2227-9717. doi: 10.3390/pr2010112.
- Ronald R. Coifman and Stéphane Lafon. Diffusion maps. *Applied and Computational Harmonic Analysis*, 21(1):5–30, July 2006. ISSN 1063-5203. doi: 10.1016/j.acha.2006.04.006.
- Felix Dietrich, Mahdi Kooshkbaghi, Erik M. Bollt, and Ioannis G. Kevrekidis. Manifold learning for organizing unstructured sets of process observations. *Chaos: An Interdisciplinary Journal of Nonlinear Science*, 30(4): 043108, April 2020. doi: 10.1063/1.5133725.
- Carmeline J. Dsilva, Ronen Talmon, C. William Gear, Ronald R. Coifman, and Ioannis G. Kevrekidis. Data-driven reduction for a class of multiscale fast-slow stochastic dynamical systems. *SIAM Journal on Applied Dynamical Systems*, 15(3):1327–1351, January 2016. doi: 10.1137/151004896.
- Carmeline J. Dsilva, Ronen Talmon, Ronald R. Coifman, and Ioannis G. Kevrekidis. Parsimonious representation of nonlinear dynamical systems through manifold learning: A chemotaxis case study. *Applied and Computational Harmonic Analysis*, 44(3):759–773, May 2018. doi: 10.1016/j.acha.2015.06.008.
- Ian J. Goodfellow, Jean Pouget-Abadie, Mehdi Mirza, Bing Xu, David Warde-Farley, Sherjil Ozair, Aaron Courville, and Yoshua Bengio. Generative Adversarial Networks. *Neural information processing systems*, June 2014. URL <https://papers.nips.cc/paper/5423-generative-adversarial-nets.pdf>. arXiv: 1406.2661.

- W. Kabsch. A solution for the best rotation to relate two sets of vectors. *Acta Crystallographica Section A*, 32(5):922–923, September 1976. doi: 10.1107/s0567739476001873.
- Diederik P. Kingma and Max Welling. Auto-Encoding Variational Bayes. *International Conference on Learning Representations*, 2014. URL <http://arxiv.org/abs/1312.6114>. arXiv: 1312.6114.
- James McQueen, Marina Meila, and Dominique Joncas. Nearly isometric embedding by relaxation. In D. D. Lee, M. Sugiyama, U. V. Luxburg, I. Guyon, and R. Garnett, editors, *Advances in Neural Information Processing Systems 29*, pages 2631–2639. Curran Associates, Inc., 2016.
- Caroline Moosmüller, Felix Dietrich, and Ioannis G. Kevrekidis. A geometric approach to the transport of discontinuous densities. *arXiv:1907.08260, accepted in SIAM-UQ*, 2020.
- Erez Peterfreund, Ofir Lindenbaum, Felix Dietrich, Tom Bertalan, Matan Gavish, Ioannis G. Kevrekidis, and Ronald R. Coifman. Loca: Local conformal autoencoder for standardized data coordinates. *arXiv 2004.07234*, 2020.
- Steven Rosenberg. *The Laplacian on a Riemannian Manifold*. Cambridge University Press, 1997. doi: 10.1017/cbo9780511623783.
- S. Rusinkiewicz and M. Levoy. Efficient variants of the ICP algorithm. *Proceedings Third International Conference on 3-D Digital Imaging and Modeling*, 2001.
- Tim Salimans, Diederik P Kingma, and Max Welling. Markov Chain Monte Carlo and Variational Inference: Bridging the Gap. *International Conference on Machine Learning*, page 9, 2015.
- Tim Sauer, James A. Yorke, and Martin Casdagli. Embedology. *Journal of Statistical Physics*, 65(3):579–616, 1991. doi: 10.1007/BF01053745.
- Ariel Schwartz and Ronen Talmon. Intrinsic isometric manifold learning with application to localization. *SIAM Journal on Imaging Sciences*, 12(3):1347–1391, January 2019. doi: 10.1137/18m1198752.
- Amit Singer and Ronald R. Coifman. Non-linear independent component analysis with diffusion maps. *Applied and Computational Harmonic Analysis*, 25(2):226–239, September 2008. ISSN 1063-5203. doi: 10.1016/j.acha.2007.11.001.
- Amit Singer, Radek Erban, Ioannis G. Kevrekidis, and Ronald R. Coifman. Detecting intrinsic slow variables in stochastic dynamical systems by anisotropic diffusion maps. *Proceedings of the National Academy of Sciences*, 106:16090–16095, 2009. doi: 10.1073/pnas.0905547106.
- Hassler Whitney. Differentiable manifolds. *The Annals of Mathematics*, 37(3):645, July 1936. doi: 10.2307/1968482.